Predicting Global Warming Impacts on Regional Water Availability

Jennifer Alltop Aminzade
Department of Earth and Environmental Sciences, Columbia University
New York, New York

David Rind
NASA Goddard Institute for Space Studies
New York, New York

Corresponding author address: Jennifer Alltop Aminzade, Department of Earth and Environmental Sciences, Columbia University, 2880 Broadway, New York, NY 10025.
E-mail: jla2126@columbia.edu

Abstract

As climate warms during the 21st century, resultant changes in water availability are an extremely important issue for society, perhaps even more important than the magnitude of warming itself. In this paper, we use the results from different climate model simulations to calculate changes in regional water availability. We examine the possibilities and problems associated with these calculations, focused on seven regions and a subset of five Atmosphere-Ocean General Circulation Models (AOGCMs) whose results were used in the 2007 IPCC report. We use two different measures of water availability changes: the modeled soil moisture and a drought index. Our results show that in some regions (Southwestern United States, Southern Europe), the models and drought measures agree on a prospective drying, while in other areas (Uruguay, Colombia, Australia) the drought index indicates drying in all three locations but there is little soil moisture change. In Eastern China, in contrast to current tendencies of flooding in the southeast and drought in the northeast, both measures show the opposite tendencies in the late 21st century. In Eastern Siberia, the drought index shows wetter conditions in winter, while the soil moisture response is mixed. Multivariate analysis demonstrates that increasing temperatures have a larger influence than changes in precipitation on 21st century drought, particularly for the drought index, in every region except Eastern Siberia. These disagreements among models and drought measures suggest that predicting changes in regional water availability remains a significant challenge.

1. Introduction

Water shortages are already an issue in many parts of the world and will become even more important in the future, as rising temperatures lead to increases in evaporation and global precipitation patterns shift (IPCC Chap. 10 2007). As temperatures increase, the amount of atmospheric water vapor increases as well. According to the Clausius-Clapeyron equation, every 1°C increase in temperature increases the water-holding capacity of the atmosphere by 7%. Higher temperatures over land relative to the ocean lead to greater relative concentrations of continental water vapor, taking more water away from the soil (Weatherald and Manabe 1999).

In addition to global warming exacerbating water shortages, growing populations and rising demand for freshwater in agriculture, industry, and energy production highlight a need for additional climate change research focused on future changes in regional water availability. Such research can inform economic and policy decisions. In order to raise awareness in areas likely to experience an increase in drought extent or severity due to global warming, we need a reliable means of quantifying the global distribution of available water on the basis of climate simulations. This is particularly crucial now with the development of phase 3 of the Coupled Model Intercomparison Project (CMIP3) database, holding the results from some 24 AOGCMs (Meehl et al. 2007). While these results offer a compelling opportunity to obtain regional projections for impact studies on future water availability, how exactly should such studies be conducted?

This paper is intended to provide a practical discussion of the current scientific consensus for 21st century drought predictions in seven focus regions. In addition, as it is impractical to expect interested parties to perform detailed analyses of output from all the AOGCMs, we use a subset of five models and two measures of future water availability. Along with comparisons provided to the averaged output from the full suite of models, this approach illustrates the possibilities and problems associated with our current ability to predict future changes in water availability on a regional level.

2. Drought Measures

There are many ways to define drought. This paper makes use of two measures: **soil moisture** and **drought index values**, specifically the Supply Demand Drought Index (SDDI; Rind et al. 1990). Obtaining the former is the more difficult of the two in practice. Soil moisture datasets are sparse and infrequently sampled, unlike the temperature and precipitation observations used to calculate drought index values; this has led the agricultural industry to rely heavily on drought indices (Robock 1998; Henderson-Sellers et al. 2002; Henderson-Sellers et al. 2003; Varis et al. 2004). Today, when using AOGCMs to model future climate, we have the variables needed to compute both drought indices and soil moisture, and both can be used for studying drought. However, there is very little agreement among models on how soil moisture is defined.

Calculating SDDI requires monthly mean precipitation and temperature as inputs for each location, but does not require regional coefficients, which are needed to calculate the commonly utilized Palmer Drought Severity Index (PDSI; Palmer 1965). While PDSI coefficients were developed mostly for the United States, SDDI can be calculated globally, and is highly correlated with PDSI in the United States (Rind et al. 1990).

Each measure has its own strengths and weaknesses. However, since SDDI and soil moisture define drought using somewhat independent methods, both are useful in understanding regional differences. Furthermore, due to a lack of observations of soil moisture, there is no way to establish which one is more realistic at this time.

3. Coupled General Circulation Model Datasets

We calculated SDDI and potential evapotranspiration using AOGCM output from two sets of simulations performed for the IPCC AR4, Climate of the 20th Century experiment (20c3m) and the SRES A2 experiment. The model consensus for the A2 scenario is global warming of approximately 3.2°C by 2100 with higher temperatures over the continents (IPCC Chap. 10 2007). The model output was provided by World Climate Research Programme's CMIP3 multi-model database (Meehl et al. 2007). Our study focused on precipitation, surface air temperature, and soil moisture output from five models: Canadian Centre for Climate Modelling and Analysis (CCCMA) Model CGCM3.1, NOAA Geophysical Fluid Dynamics Laboratory (GFDL) Model CM2.1, Goddard Institute for Space Studies (GISS) Model E_r, Hadley Centre for Climate Prediction Model HadCM3 (HADCM3), and University of Tokyo Center for Climate System Research Model 3.2 medium resolution (MIROC). The years 1901 to 2000 were taken from the Climate of the 20th Century experiment, and the years 2001 to 2100 from the A2 scenario. From the HADCM3 model, the years were shifted 1 year earlier (1900-1999 and 2000-2099) due to available output. These five models can be considered representative of the 24 CMIP3 models in two pertinent areas for studying drought. They represent a range in land surface parameterizations and a range of skill in simulating El Niño Southern Oscillation (ENSO) interdecadal variability (Lin 2007).

4. Global Comparison of Drought Measures

We compared SDDI and soil moisture to determine the relative abilities of the two measures to estimate future shortages or abundances of water globally. All five AOGCMs show significant drying trends in 21st century SDDI compared to the 20th century, while both SDDI and soil moisture trends show the extent of land area in severe drought conditions more than tripling in the next century. Dry areas are getting drier, wet areas are getting wetter, and both are expanding according to both SDDI and soil moisture for all models, as shown in Figure 1.

Model projections of the change in surface air temperature over land (excluding Antarctica and Greenland) by the year 2100 range from 4° to 6° C above the 1971 to 2000 average. Observed global averages in the 20th century agree well with modeled temperature change. Over land, some models show steady increases in precipitation over the 21st century and others exhibit only minor increases. Globally, all five models show increasing precipitation over land ranging from 1.5 to 6 mm/day by the year 2100.

Over the next 100 years, global-average SDDI predictions over land steadily decrease, indicating severe drying globally by the year 2100. In contrast, global-average soil moisture projections show almost no change in the 21st century in all models except the HADCM3 model, which shows a steady decrease. However, both SDDI and soil moisture do agree that in all models the percentage of gridboxes experiencing both extreme drought and extreme fluvial conditions at the 5% level continues to increase over the next century. This increase in dry and wet extreme conditions is approximately equal for soil moisture in the four models resulting in very little change in the global-average. In the SDDI analysis, extreme drought outweighs extreme fluvial conditions although

both do increase, which explains why global-average SDDI shows an overall drying trend. Because raw SDDI and soil moisture values give little intuitive understanding of the of the severity of drought, Figure 1 displays the severity of water availability relative to prior conditions, as a percentage of time during which those conditions occurred in the past. For example, 3% drought indicates a drought of a severity seen during only 3% of the control time period. Using 1928-1978 as our control period allows us to express SDDI and soil moisture during 2071-2100 in terms of such percentages.

5. Global comparisons of AOGCM climate predictions relevant for water availability

In addition to conflicts between drought measures, another source of potential disagreement for future projections comes from the AOGCMs themselves. Table 1 shows the percentage agreement between the five AOGCMs we considered, expressed as the percentage of grid boxes for which five models agreed on the direction of change of various climate measures. We conducted this grid box-to-grid box comparison by interpolating the grids of four of the models to the size of the model with the coarsest resolution, a 4° by 5° grid. Considering all of the land grid points for the five AOGCMs, there is 100% agreement on the sign of the temperature change (warming) between the end of the 21st and the 20th centuries for scenario A2. The agreement drops to 47% when considering precipitation changes, and to only 14% for soil moisture (i.e., the five models agree on the sign of soil moisture change in only 14% of the grid boxes). The SDDI change is in better agreement (58%).

During mid-latitude summer-time droughts, there is currently a strong anti-correlation between the sign of temperature and precipitation changes. Such droughts are

synoptic in nature, characterized by a mid-tropospheric anti-cyclone providing for descent, cloud free conditions, warm temperatures, and little rainfall. In contrast, our analyses show only 11% of the grid boxes in the five AOGCMs sharing this inverse relationship on the annual average; 36% have both temperature and precipitation increases in the five models, with global warming producing both increased temperature (and evaporation) along with precipitation. These changes compete against one another in their influence on soil moisture, helping to explain the minimal agreement on the sign of soil moisture changes. There is unanimity on the sign of the precipitation and soil moisture changes in only 8% of the grid boxes, and complete agreement on the inverse relationship between temperature and soil moisture in only 12%. In contrast, the models show much more commonality for the sign of the temperature and SDDI changes (52%), suggesting temperature change is its dominant factor via influence on potential evaporation. With disagreement on the sensitivity of these two water availability indicators to meteorological forcing, it is thus not surprising that all the models show the same sign of SDDI and soil moisture change in only 12% of the grid boxes (due primarily to their disagreement on soil moisture). In effect, considering just these five models, in only 1 out of every 8 grid boxes is there a unanimous indication of even the sign of future water availability change.

6. Regions of Interest

We chose seven regions for closer study: Southwestern United States, Southern Europe, Uruguay, Colombia, Eastern China, Eastern Siberia, and Australia. With the exception of Eastern Siberia, these are regions with large populations that are vulnerable to changes in water availability. The seven regions were chosen based on one of three

criteria: 1) likelihood for increased drought severity significantly affecting local way of life, 2) uncertainty of drought due to disagreement among models, or 3) disagreement in soil moisture and drought index trends. Listed below are summaries of relevant climate features in each of these regions.

As our intent is to explore whether meaningful predictions are possible on a regional scale, we are concerned with both aspects of potential variability: differences among models, and differences between water availability measures.

a. Southwestern United States (Arizona, Southern California, Colorado, Nevada, New Mexico and Utah)

The Southwestern United States is an area with a current scarcity of water and a history of battling drought. The estimated population in the Southwestern U.S. as of 2007 was approximately 55 million with an estimated annual population growth ranging from 0.84% to 2.93% (U.S. Census Bureau 2008). Utah, Arizona and New Mexico have the top three highest population growth rates in the United States. Consumption is not likely to stay steady with population increases unless major water conservation projects are successful. In addition, even at current consumption, Lake Mead and Lake Powell, the two major reservoirs in the Colorado River Basin, are in danger of drying up within the next fifty years (Barnett et al. 2008). Energy shortages are a potential threat when levels in Lake Mead and Lake Powell drop, as these two lakes provide the majority of hydroelectric power in the region.

The Southwestern U.S. and Northwestern Mexico receive a large portion of their annual precipitation from the North American Monsoon System (NAMS) in the summer.

ENSO exerts a large influence on drought in the Southwestern U.S. during the boreal winter, with greater (less) rainfall during El Niño (La Niña). IPCC AR4 multi-model averages show a future decrease in annual precipitation in the Southwestern U.S. and a weakening of the North American Monsoon System. The decrease is due to a predicted increase in the land-ocean temperature gradient during summer, and an amplification and northward displacement of the subtropical anticyclone (IPCC Chap. 10 and 11 2007). There is no agreement on the likely change in ENSO phase or background SST conditions in the tropical Eastern Pacific.

We used output from five AOGCMs to compute the predicted temperature and precipitation differences between the last 30 years of the 21st and 20th centuries assuming the IPCC scenario A2 for future warming (Table 2). Temperature differences ranged from 4.5°-6.5°C in the summer and 2°-5.2°C in the winter months. For summer months, four of the five models agreed that there will be less precipitation, ranging from a 9%-44% decrease from the control (1928-1978) average. Both the SDDI and the soil moisture predictions agreed that summer months will see significant drying due to increased temperatures and evapotranspiration, and an almost unanimous decrease in precipitation and cloud cover. Winter months showed disagreement among models in soil moisture, which reflects their mixed predictions for future precipitation. However, SDDI values all showed continued drying in DJF. The average degree of summer drought predicted in the 21st century is equivalent to the severity that occurred every 9±7 years in the 20th century according to SDDI, or 2.4±1.7 years according to soil moisture.

b. Southern Europe (Portugal, Spain, France and Italy)

Currently, Italy and Spain can be described as water-stressed based on their Water Exploitation Indices (WEI). The WEI is the total water abstraction divided by the long-term available annual resource, and a country is deemed water-stressed when its WEI is above 20% (European Environment Agency 2008). Spain has the highest water stress in Southern Europe with a WEI of 33%. Italy is not far behind with a WEI of 24%, while France and Portugal are close to the water-stress threshold, with WEI values of 18% and 15% respectively. The economies of Southern Europe are heavily dependent on industries that are vulnerable to water risks, with 55% to 70% of Southern Europe's major industries falling into this category (CIA 2008). 74% of total annual freshwater withdrawals in France are used for industrial purposes. There are hundreds of water treaties and agreements currently in place between these countries and with other European nations to protect and clarify water rights, particularly with respect to surface waters, which cross or outline borders (Oregon State University 2008). There are additional treaties in effect that concern the sharing of hydroelectric energy, since all three nations are dependent on hydroelectric power generation for a significant fraction of total energy use.

Variations in the wintertime North Atlantic Oscillation (NAO) impact precipitation levels over Southern Europe, with drier conditions during the more positive phase (Hurrell and Van Loon 1997). The NAO has been found to influence water availability not only in winter, but all year long in Southern Europe (Lopez-Moreno and Vicente-Serrano 2008).

The IPCC AR4 finds that Southern Europe has already experienced annual precipitation trends ranging from a 20% decrease to a 20% increase per century between 1901 and 2005, and observed temperature changes ranging from 0.25°-0.55°C per decade between 1979 and 2005 (IPCC Chap. 3 2007). Heat waves in Southern Europe have received a lot of attention, particularly after the severe heat wave during the summer of 2003, which has been cited as the cause of approximately 20,000 deaths in the region (Met Office 2008). The IPCC AR4 found that annual temperatures in Europe are likely to increase more than the global mean (IPCC Chap. 11 2007). The multi-model ensemble projects a decrease in precipitation over all of Southern Europe in JJA by the last 20 years of the 21st century (IPCC Chap. 10 2007). Consistent with this result, Stephenson et al. (2006) examined 15 Coupled Model Intercomparison Project (CMIP2) models with the ability to simulate the NAO pressure dipole and found that 13 predict a shift to a more positive NAO index as CO_2 concentrations increase. In addition, the model simulations show that the snow season is very likely to shorten in all of Europe due to warmer temperatures, and snow depth is likely to decrease in most of Europe, resulting in changes in the seasonality of snowmelt runoff.

According to the five IPCC models we studied, wintertime increases in temperature are likely to be smaller than summertime increases (Table 3). The difference in average DJF temperature between the last 30 years of the 20th century and the last 30 years of the 21st century ranged from 2.53°-3.51°C. Model projections for JJA temperature changes ranged from 4.87°-6.63°C. Four out of five of the models showed precipitation decreases in JJA ranging from 25.2%-57.1% of the JJA average for the last 30 years of the 20th century. On the other hand, wintertime precipitation showed increases

in all but one of the five models in Table 3, which amounts to a 1%-9.5% increase from the 1971-2000 DJF mean. This is different from the full IPCC AR4 scenario A1B multi-model ensemble, which projected decreased precipitation in Portugal, Spain and Italy in DJF by the years 2080-2099 (IPCC Chap. 10 2007).

In both summer and winter, all models studied projected a decrease in soil moisture and SDDI (Table 3). The projected soil moisture values showed the smallest changes. Dry conditions, which occurred only once every 1.02-1.59 years in winter months between 1971 and 2000, are projected to be the average state by 2071-2100 winter months. During summer, average dry conditions are projected to increase to what occurred one year in every 1.66-4.71 years during the 1971-2000 period. SDDI values showed a much stronger drying trend, with wintertime average conditions that only occurred once every 3.39-8.60 years between 1971 and 2000. Average summertime conditions in the 2071-2100 time period are projected to mirror conditions that occurred only once every 4.55-12.44 years in the 1971-2000 period.

c. Uruguay

Uruguay's current abundance of water has shaped both its public and private sectors. Large dams along the Uruguay and Negro Rivers, designed to generate hydroelectric power, provide 17.3 km^3 of storage capacity, approximately 5.5 times Uruguay's total annual freshwater withdrawal (AQUASTAT 2008; CIA 2008). The CIA estimates that 99.1% of Uruguay's total energy production is hydroelectric (CIA 2008), and in 2007, Uruguay exported an estimated 1 billion kWh of electricity (CIA 2008). An additional 40,000 km^3 of freshwater lies beneath Uruguay, Brazil, Argentina and

Paraguay in the Guarani aquifer, one of the largest groundwater reserves in the world (AQUASTAT 2008). Increases in population are unlikely to be a strain on future water supplies (CIA 2008), leaving the export industry as their only potential threat. Hydroelectric power and water-intensive crops such as rice make up a significant portion of Uruguay's exports.

Weather variations in Uruguay are generally linked to ENSO, with more precipitation in December, January and February (DJF) during El Niño events. The same phase leads to warmer temperatures in June, July and August (JJA). La Niñas are linked to drier conditions in JJA. The Antarctic Oscillation (AAO) is also potentially linked to weather conditions in Uruguay, although the influence is still unclear. Silvestri and Vera (2003) report negative correlations between the AAO index and precipitation in November and December (late spring) and positive correlation in July and August (late winter). A more recent study by Gillett et al. (2006) was unable to find a robust response.

The majority of the models used with the IPCC AR4 A1B scenario project increases in Uruguay's precipitation between the last 20 years of the 20th century and last 20 years of the 21st century. Of the 21 models, 14-18 agree on this prediction in DJF and 8-16 agree in JJA (IPCC Chap. 11 2007), despite the fact that the models disagree on the future behavior of ENSO (IPCC Chap. 11 2007).

Based on the IPCC A2 scenario in the five models we studied, we see a temperature increase ranging from 1.5°-3°C in JJA, and 2.3°-3.1°C in DJF by the end of the 21st century (Table 4). Precipitation predictions are inconsistent between models during winter (JJA), but in summer all show an increase in rainfall ranging from 4%-22% compared to the average of last 30 years of the 20th century.

Soil moisture projections show conditions in both seasons that are only slightly wetter than those of the control period, 1928-1978, with only the MIROC model in disagreement (Table 4). In contrast, changes in the SDDI show significant drying in all five models for both winter and summer.

There is currently very little consensus among models about how climate will change in Uruguay. Precipitation, soil moisture, and SDDI all give different pictures of future water availability in the region. The most likely cause of these discrepancies is the inability of most models to depict a realistic ENSO.

d. Colombia

While Colombia's total annual renewable water resources (TARWR) are abundant, totaling about 200 times its annual freshwater withdrawals (Molden 2007), it has minimal infrastructure in place for water storage. As of 2000, Colombia had only 9.1 km^3 of reservoir storage, less than the annual freshwater withdrawals of 10.71 km^3 (AQUASTAT 2008). Due primarily to the vast amount of available water, Colombia has become heavily dependent on hydroelectric power generation. Hydroelectric power accounts for 72.7% of Colombia's total energy production, and in 2005, Colombia exported 1.758 billion KWh of electricity (CIA 2008). Many of Colombia's major industries are also dependent on a large quantity of water or are vulnerable to changes in water availability (Morikawa 2007).

Agriculture officially accounts for only 11.5% Colombia's GDP (CIA 2008). However, that figure does not include profits from illegal drug trade. As of 2006, an estimated 62% of world cocaine production came from Colombia. With approximately

78,000 hectares of coca plants valued at US$13,039/hectare for cocaine hydrochloride, the cocaine grown each year in Colombia has an estimated worth of over a billion US dollars (United Nations 2007). In addition to coca, Colombia is also known to grow cannabis and opium poppies.

Future increases in Colombia's population are unlikely to strain its water supplies (CIA 2008). The largest potential loss is to the export industry, since limited water availability would affect hydroelectric power exports and agricultural products. Changes in water availability could even affect the world drug trade if Colombia were no longer able to continue producing at the same volume. In addition, Colombia's lack of water treaties with any of its neighboring countries puts the country at high risk for potential water conflicts

Climate in Colombia is intimately tied to ENSO patterns. El Niño is associated with low rainfall and discharges, and La Niña is strongly associated with higher precipitation and streamflows (Poveda and Mesa 1997). The disagreement among models on the future behavior of ENSO thus influences projections for Colombia (IPCC Chap. 11 2007). Nevertheless, the IPCC AR4 A1B scenario multi-model ensemble for the precipitation changes from 1980-1999 to 2080-2099 indicate that the there will be increases in precipitation in Southwestern Colombia in all seasons and there will be drying in the north annually, particularly during JJA (IPCC Chap. 11 2007). Colombia's southwestern half shows much higher agreement among models, with more than 8 models out of 21 agreeing in all seasons (IPCC Chap. 11 2007).

Based on the IPCC A2 scenario in the five models we studied, Colombia will see a temperature increase ranging from 2.85°-6.25°C in JJA by the end of the 21st century

(Table 5). In DJF, there is a projected increase in temperature ranging from 2.95°-4.85°C. In both JJA and DJF there is general agreement in sign between the models on precipitation predictions averaged across the region. Among the five models we examined, four models show a decrease in rainfall in JJA ranging from 4.6%-35.85% compared to the average of the last 30 years of the 20th century. In DJF, four models predict a precipitation increase, with projected changes ranging from a decrease of 1.1% to an increase of 27.0%. The five models are thus in general agreement with the multi-model A1B assessment.

Changes in soil moisture show conditions that are close to those of the control period (1928-1978) in DJF and JJA (Table 5). However, changes in SDDI show significant drying in four out of five models for both JJA and DJF. In JJA, the average conditions at the end of the 21st century mirror drought conditions that occurred only once every 1.07-4.54 years at the end of the 20th century. In DJF, conditions at the end of the 21st century occurred once every 1.04-7.80 years in the last 30 years of the 20th century.

In summary, there is general agreement among models on Colombia's future precipitation trends, but soil moisture and SDDI give different pictures of future water availability. As was the case with Uruguay, this conflict can be attributed to the inability of most models to depict a realistic ENSO.

e. Eastern China

Eastern China is defined as the Chinese provinces east of Tibet and south of Inner Mongolia. In general this region has abundant water resources: as of 2005, China's

TARWR were approximately 2,830 km^3 per year, of which only about 19% (550 km^3 per year) is used (Water 2006). Domestic, industrial and agricultural freshwater withdrawals are approximately 7%, 26%, 68% respectively (CIA 2008), so both food and production would be affected by water availability changes.

China has recently invested heavily in and become dependent on hydroelectric power generation, which requires the maintenance of minimum water levels. Total hydroelectric output in 2007 was approximately 602,360 thousand MWh, which represents about 18.5% of China's total power production (CIA 2008). With the construction of the Three Gorges Dam, the largest hydroelectric power station in the world, China will add 22,500 MW to its generating capacity, representing an annual energy generation capacity of more than 100 billion kWh when fully operational (CTGPC 2009).

Eastern China's climate is heavily influenced by the Asian Monsoon, with much greater rain in summer than winter, although this is not as true near the coast, which receives significant rain in winter as well. Precipitation observations have shown no clear trends on a national level (IPCC Chap. 3 2007). However, there has been a pattern of increased rainfall in the southeast and decreased rainfall in the northeast, often called the "southern flooding and northern drought" pattern. This pattern has caused extensive and severe flooding in the Yangtze River valley, droughts in the north, and drying up of the Yellow River. These changes in precipitation are linked to a weakening trend in the East Asian summer monsoon since the 1920s (Allan and Ansell 2006), consistent with a tendency for a southward shift in the summer rain belt over Eastern China (Zhai et al. 2004). The monsoonal changes in turn have been related to SST variations in the eastern

tropical Pacific and the tropical Indian Ocean (Gong and Ho 2002) and potentially upper tropospheric/lower stratospheric cooling (Yu et al. 2004).

ENSOs also impact this region (Chang 2004, Lau et al. 2006; McBride et al. 2003, Wittenberg et al. 2006), with El Niños (La Niñas) suppressing (enhancing) the winter monsoon (Lau et al. 2006; Chang 2004) but increasing summer precipitation, at least partly due to their influence on tropical storms (Camargo and Sobel 2004; Wu et al. 2004). Recent years have seen many changes in tropical storm and typhoon characteristics. In the Western Pacific, the number of category 4 and 5 tropical storms is approximately 36% higher for the years 1990-2004 than the years 1975-1989 (Webster 2005).

IPCC AR4 models suggest that global warming will alter China's land-sea temperature contrast, weakening the winter monsoon and strengthening the summer monsoon (Kimoto 2005). The IPCC AR4 A1B scenario multi-model ensemble for the precipitation changes from 1980-1999 to 2080-2099 indicates that China will experience increasing annual precipitation between 0% and 20%. In the boreal winter, precipitation changes range from a 5% decrease in Southeastern China up to a 50% increase in Northeastern China, in what appears to be a modification or possible suppression of the "southern flooding and northern drought" pattern. In the summer, precipitation predictions range between a 0% and 15% increase, and no north-south pattern arises (IPCC Chap. 11 2007).

The five models we studied predict a temperature increase in JJA ranging from 2.73°-4.43°C by the end of the 21st century (Table 6). In DJF, there is a projected increase in temperature ranging from 3.15°-4.19°C. In both JJA and DJF there is general

agreement in sign between the models on precipitation predictions averaged across the region. In JJA, all five models show an increase in rainfall ranging from 0.8%-16.6% compared to the average of the last 30 years of the 20th century. In JDF, four of the models show an increase, with projected changes varying across a wide range, from -4.1% to +35.1%. Changes in soil moisture show conditions that are relatively close to those of the control period (1928-1978) in DJF and JJA averaged across the entire region (Table 6). The same is true with changes in the SDDI for both JJA and DJF.

However, all five models show significant water availability variability within Eastern China on a smaller scale during winter and summer. Our findings agree with the IPCC AR4 findings summarized above. In all five of the models we studied there is a north-south division in one or both drought measures. In the majority of cases, the models predict a decrease in water availability by the end of the 21st century in Southeastern China and an increase in Northeastern China. This trend would oppose the current "southern flooding and northern drought" pattern in China.

The future influence of ENSO on the climate of Eastern China remains to be determined. IPCC AR4 models show very little consistency in tropical storm changes in the Western Pacific, likely due to inconsistencies in ENSO. Higher resolution models project increases in precipitation intensity due to future tropical cyclones. Some of these models also project increases in tropical storm peak wind intensities.

f. Eastern Siberia

Due to its minimal development, the societal impacts of water availability changes in Siberia would be small at a regional level. However, Siberia has the ability to

impact the globe through large methane emissions associated with permafrost melting. Permafrost is a major carbon reservoir: Siberia and Alaska are estimated to contain approximately 500 Gt of carbon in frozen yedoma (Pleistocene-age loess permafrost), approximately 400 Gt of carbon in non-yedoma permafrost, and between 50 and 70 Gt of carbon in Western Siberian peatbogs (Zimov et al. 2006).

Northern Siberia lakes are also a larger source of atmospheric methane than previously thought. Between 1974 and 2000, the expansion of thaw lakes in Northern Siberia has been linked to a 58% increase in lake methane emissions (Walter et al. 2006). Fortunately, if Siberia gets wetter as well as warmer, the growth of natural vegetation would draw CO_2 from the atmosphere, helping to limit the growth in its contribution to greenhouse capacity. The mean changes projected by the IPCC models for the A1B scenario show increased rainfall, but on average small decreases in soil moisture, with much inter-model variability (IPCC 2007).

Based on the five A2 scenario AOGCMs, the projected increase (over the 1971-2000 average) in Eastern Siberian temperatures by the end of the 21st century ranges from 1.73°-5°C in JJA and 4.51°-8.98°C in DJF. Strong high latitude warming is likely to melt large portions of permafrost (IPCC Chap. 10 2007).

Siberia is also predicted to receive far more precipitation by the end of the 21st century. Projections from the five focus AOGCMs estimate JJA precipitation increases ranging from 7.1%-30% above the control (1928-1978) average and even more dramatic DJF increases ranging from 27.8%-63.1% above the control average.

Increased precipitation and temperatures tend to compensate in their impact on both the SDDI and soil moisture values. For both drought measures, projected conditions

change very little on average by the end of the 21st century. DJF is projected to be wetter by all models for SDDI and by three out of the five models for soil moisture. JJA conditions are projected to by slightly drier by the majority of models for both drought measures. Naturally, with such large temperature increases, the percentage of precipitation falling as snow or ice versus water will change, favoring reduced water availability for later in the growing season from this effect.

g. Australia

Australia is a climatically diverse country with a tropical climate in the north, a dry climate in the western and central regions, and a temperate climate on the eastern coast, which is home to a large percentage of the national population. There is a great deal of variation in annual rainfall between Australia's regions. Drought is a yearly reality in many areas; the deserts in Central and Western Australia receive on average less than 250 mm per year of rainfall. In contrast, annual average rainfall in some tropical areas is sometimes in excess of 2,500 mm (AGNWC 2008). The high average rainfall in the north is in part due to the summer monsoon and tropical cyclones between December and April. The temperate regions receive rain in all seasons.

Australia's TARWR are close to 492,000 GL (Water 2006). However, annual water use is only 24.06 GL, about 5% of the TARWR. Although Australia is the driest habitated continent, it offers great potential for renewable water capture and storage. As of 2005, Australia had the ability to store 83,853 GL of water and was close to half capacity with 39,959 GL (CIA 2008).

The Australian monsoon season occurs during the austral summer. The strength of the monsoon is variable from year to year, and is highly influenced by ENSO, MJO, and tropical cyclone activity (Kullgren and Kim 2006; IPCC Chap. 3 2007). During warm phase ENSO years in June, July and August, Eastern Australia typically experiences anomalously dry conditions. Although the drought in 2009 occurred during a La Niña, La Niñas will generally act to prolong the duration of the monsoon (Kim et al. 2006). While the influence of MJO on the monsoon is small compared to the influence of ENSO, Kim et al. (2006) find that the MJO plays a major role in the onset and termination of the monsoon.

Cyclone activity is also associated with ENSO. In Australia, above average tropical cyclone seasons are typical of La Niña years, while below average tropical cyclone activity is associated with El Niño (Plummer et al. 1999; Kuleshov and de Hoedt 2003; IPCC Chap. 3 2007).

According to the IPCC AR4, Australia will experience warming similar to the global average (IPCC Chap. 11 2007). The Australian monsoon is projected to increase in intensity during the southern summer, likely due to the fact that the continental-scale land-sea thermal contrast will become larger (IPCC Chap. 10 2007). Models also project an increase in peak wind intensities and increased near-storm precipitation in future tropical cyclones (IPCC Chap. 10 2007). This would bring more precipitation in the summer. However, there is disagreement among models on the future behavior of ENSO, which heavily influences the Australian monsoon and tropical cyclones in the region (IPCC Chap. 11 2007). The models are also unclear on the future characteristics of the Inter-decadal Pacific Oscillation, which has a weak negative correlation with the

monsoon (IPCC Chap. 3 2007), and the Indian Ocean Dipole, which is negatively correlated with rainfall over Australia (Ashok et al. 2003).

Looking at individual climate regions of Australia, the AR4 finds that precipitation is likely to decrease in Southern Australia in winter and spring and in Southwestern Australia in winter. This decrease in precipitation is at least partially due to the poleward expansion of the Hadley Cell over Australia. There is no agreement among models about precipitation changes in Northern or Central Australia (IPCC Chap. 10 2007).

Based on the five models we studied in the AR4, using the IPCC A2 scenario, we will see a temperature change ranging from a 3.09°-4.26°C increase in JJA by the end of the 21st century (Table 8). In DJF, the southern summer, the models project an increase in temperature ranging from 3.33°-4.1°C.

Precipitation predictions are inconsistent between models when averaged across the continent. Among the five models examined, three models show a rainfall decrease in JJA and two models show an increase. In DJF, two models show a rainfall decrease and three show an increase. Changes in soil moisture show no clear trend (Table 8). However, changes in the SDDI show drying in five out of five models for both winter and summer. In summer, the drying is more severe, with average conditions at the end of the 21st century similar to drought that occurred only once in every 4.32-6.97 years at the end of the 20th century. If conditions in Australia continue to get drier, the chance of bushfires will increase, likely resulting in fires even more widespread than those of 2009.

7. Discussion

As we saw in the preceding sections, there is frequent disagreement in predictions of future water availability, both between *climate models* and between the *drought measures* computed from those models. Understanding the reasons for the former type of disagreement, and reconciling the differences between climate models, is an important topic for future research, but is beyond the scope of this paper. Instead, we will focus the remainder of our analysis on understanding the latter type of disagreement, and explaining the discrepancies between drought measures.

As both of the measures we used are influenced by predicted temperature and precipitation changes, we can express their relative influence as a linear relationship:

$$\Delta(SM) = \beta_C + \beta_T(\Delta T) + \beta_{PR}(\Delta Pr) \quad (1)$$

$$SDDI = \beta_C + \beta_T(\Delta T) + \beta_{PR}(\Delta Pr) \quad (2)$$

where β_C,β_T, and β_{PR} are derived coefficients, SM is soil moisture, T is surface temperature, Pr is precipitation and all anomalies are relative to control (1928-1978) averages.

Based on these linear equations, we calculated multiple linear regressions for each of our seven focus regions using annual, JJA and DJF SDDI and soil moisture values, from the years 1901-2100. We found that the best-fit coefficients β_T and β_{PR} were generally of the same order of magnitude when performing soil moisture regressions, while β_T was commonly much larger than β_{PR} for SDDI regressions. This suggests that temperature exerts a far greater influence on SDDI than precipitation, while temperature and precipitation contribute more evenly to soil moisture predictions.

Nevertheless in all regions, regression analysis (Table 9a, 9b) showed that temperature has a larger influence than precipitation on both SDDI and soil moisture ($\beta_T > \beta_{PR}$) with only three exceptions, the annual soil moisture regression for the Southwestern U.S., the annual soil moisture regression for Uruguay, and the annual and DJF SDDI regressions for Eastern Siberia. In Eastern Siberia, annual and DJF SDDI values are more heavily influenced by precipitation, while soil moisture values show a stronger temperature influence. The r^2 values (Table 9a, 9b) we computed during our regressions indicate that a highly significant portion of the variance in both soil moisture and SDDI can be explained by the linear relationship to temperature and precipitation changes.

For drought indices, temperature acts through a formulation associated with potential evapotranspiration (EP). The SDDI (like the PDSI) uses the Thornthwaite EP. To assess the sensitivity of the result to that formulation, we repeated our calculations with the Penman EP, and came up with very similar results.

The true sensitivity of evaporation to increasing temperature, in both drought indices and calculations affecting soil moisture in GCMs, remains a challenging problem for future study, with the importance of absorbed sunlight receiving emphasis at least at a global scale (e.g., IPCC 2007). Nevertheless, the PDSI, whose changes with climate are very similar to that of the SDDI (Rind et al. 1990), has been shown to be a good indicator of drought changes over the past 1000 years as estimated from tree-ring analysis (Cook et al. 2004).

Today's water availability deficits invariably result from decreased precipitation, but in the future this may no longer be the case. Future droughts may occur primarily

because of temperature increases, and may even feature increased precipitation. To evaluate how the absence of the strong warming trend present in the 21st century simulations would affect our regression results, we performed an additional analysis for the 20th century with one model, GFDL. We found that temperature was still clearly a larger influence on all regions annually, in summer, and in winter, except for in Siberia, and the importance of temperature relative to precipitation was still found to be larger in SDDI calculations than in calculations of soil moisture.

8. Conclusions

Over the next century, rising temperatures and changes in precipitation over land will influence water availability across the globe. The development of the CMIP3 database made more generally available the model projections needed to estimate future water availability at a regional level. In this paper, we described our experience in using five different models and two measures of water availability to predict changes in water availability for seven regions.

Two regions, the Southwestern U.S. and Southern Europe, show agreement among models and between drought measures, all of which predict that water availability will decrease over the next century. Three other regions, Colombia, Australia and Uruguay, show little change in soil moisture despite model disagreements concerning future precipitation trends in the latter two countries (at least in part associated with different ENSO phase forecasts). The opposing influences of temperature and precipitation, combined with their different projected warming magnitudes, are enough to provide for similar, unchanging, soil moisture responses. However, for these same

regions, there is agreement among all models in both summer and winter for more negative SDDI values, indicating drier conditions throughout the 21st century.

In Eastern China, the models predict increases in overall precipitation and warmer temperatures, resulting in little water availability change, according to both soil moisture and SDDI. However, on a smaller scale within China, there is a projected increase in water availability in Northeastern China and a corresponding decrease in Southeastern China. Siberia is the only region in which all models agree that SDDI will indicate more fluvial conditions by the end of the 21st century in DJF, and the only region where SDDI is more influenced by precipitation than by temperature. However, the models disagree in Siberia on their soil moisture response.

Disagreements between models and drought measures make it difficult to predict the future of water availability with great certainty. Nevertheless, we believe it is valuable to characterize water availability to the best degree to which our models and measures are capable. Doing so helps us understand the disagreements between predictions, which is an essential first step towards reconciling conflicts between models and measures. Modelers are currently preparing for the CMIP4 simulations; we look forward to learning whether it offers greater convergence in regional predictions and water availability measures.

Acknowledgments.

Climate Modeling at NASA Goddard Institute for Space Studies is supported by the NASA Climate Change focus area.

References

Allan, R.J., and T. Ansell, 2006: A new globally complete monthly historical gridded mean sea level pressure data set (HadSLP2); 1850–2003. *J. Clim.*, **19**, 5816–5842.

AQUASTAT, cited 2008: AQUASTAT. Translated to English by Google. [Available online at http://www.fao.org/nr/water/aquastat/countries/colombia/indexesp.stm.]

Ashok, K., Z. Guan, and T. Yamagata, 2003: Influence of the Indian Ocean Dipole on the Australian winter rainfall, *Geophys. Res. Lett.*, **30**, 1821, doi:10.1029/2003GL017926.

Australian Government National Water Commission (AGNWC), cited 2008: Australian Water Resources 2005. [Available online at http://www.water.gov.au/.]

Barnett, T.P., D.W. Pierce, H.G. Hidalgo, C. Bonfils, B.D. Santer, T. Das, G. Bala, A.W. Wood, T. Nozawa, A.A. Mirin, D.R. Cayan, and M.D. Dettinger, 2008: Human-induced changes in the hydrology of the western United States. *Science*, **319**, 1080-1083.

Camargo, S.J., and A.H. Sobel, 2004: Western North Pacific Tropical Cyclone Intensity and ENSO. Technical Report No. 04-03, International Research Institute for Climate Prediction, Palisades, NY, 25 pp.

Central Intelligence Agency (CIA), cited 2008: The World Factbook. [Available online at https://www.cia.gov/library/publications/the-world-factbook/.]

Chang, C.-P., Ed., 2004: East Asian Monsoon. World Scientific Series on Meteorology of East Asia, Vol. 2, World Scientific, 564 pp.

China Three Gorges Project Corporation (CTGPC), cited 2009: China Three Gorges Project Corporation. Translated from Chinese to English by Google Translate.

[Available online at http://www.ctgpc.com.cn/sx/news.php?mNewsId=30559.]

Cook, E. R., C. A. Woodhouse, C. M. Eakin, D. M. Meko, and D. W. Stahle, 2004: Long-term aridity change in the western United States. *Science*, **306**, 1015-1018.

European Environment Agency, cited 2008: European water resources. [Available online at http://www.eea.europa.eu/themes/water/water-resources/.]

Gillett, N. P., T. D. Kell, and P. D. Jones, 2006: Regional climate impacts of the Southern Annular Mode. *Geophys. Res. Lett.*, **33**, doi:10.1029/2006GL027721.

Gong, D.Y., and C.-H. Ho, 2002: Shift in the summer rainfall over the Yangtze River valley in the late 1970s. *Geophys. Res. Lett*., **29**, doi:10.1029/2001GL014523.

Henderson-Sellers, A., A.J. Pitman, P. Irannejad, and K. McGuffie, 2002: Land-surface simulations improve atmospheric modeling. *Eos, Trans. Amer. Geophys. Union,* **83,** 145–152.

Henderson-Sellers, A., P. Irannejad, S. Sharmeen, T.J. Phillips, K. McGuffie, and H. Zhang, 2003: Evaluating GEWEX CSEs' simulated land-surface water budget components. *GEWEX News,* Vol. 13, No. 3, International GEWEX Project Office, Silver Spring, MD, 3–6.

Hurrell, J. W., and H. Van Loon, 1997: Decadal variations in climate associated with the North Atlantic Oscillation. *Climatic Change,* **36,** 301–326.

IPCC, 2007: Climate Change 2007: The Physical Science Basis. Contribution of Working Group I to the Fourth Assessment Report of the Intergovernmental Panel on Climate Change [Solomon, S., D. Qin, M. Manning, Z. Chen, M. Marquis, K.B. Averyt, M. Tignor and H.L. Miller (eds.)]. Cambridge University Press, Cambridge, United Kingdom and New York, NY, USA, 996 pp.

Kim, K.-Y., K. Kullgren, G.-H. Lim, K.-O. Boo, and B.-M. Kim, 2006: Physical mechanisms of the Australian summer monsoon: 2. Variability of strength and onset and termination times, *J. Geophys. Res.*, **111**, D20105, doi:10.1029/2005JD006808.

Kimoto, M., 2005: Simulated change of the east Asian circulation under global warming scenario. *Geophys. Res. Lett.*, **32**, L16701, doi:10.1029/2005GL023383.

Kuleshov, Y., and G. de Hoedt, 2003: Tropical cyclone activity in the Southern Hemisphere. *Bull. Aust. Meteorol. Oceanogr. Soc.*, **16**, 135–137.

Kullgren, K., and K.-Y. Kim, 2006: Physical mechanisms of the Australian summer monsoon: 1. Seasonal cycle, *J. Geophys. Res.*, **111**, D20104, doi:10.1029/2005JD006807.

Lau, N.C. and M.J. Nath, 2006: ENSO modulation of the interannual and intraseasonal variability of the East Asian monsoon - A model study. *J. Clim.*, **19**, 4508-4530.

Lin, J.-L., 2007: Interdecadal variability of ENSO in 21 IPCC AR4 coupled GCMs, *Geophys. Res. Lett.*, **34**: L12702, doi:10.1029/2006GL028937.

Lopez-Moreno, J.I. and S.M. Vicente-Serrano, 2008: Positive and negative phases of the wintertime north Atlantic oscillation and drought occurrence over Europe: A multitemporal-scale approach. *J. Clim.*, **21**, 1220-1243.

McBride, J.L., M.R. Haylock, and N. Nicholls, 2003: Relationships between the Maritime Continent heat source and the El Niño-Southern Oscillation phenomenon. *J. Clim.*, **16**, 2905–2914.

Meehl, G.A., C. Covey, T. Delworth, M. Latif, B. McAvaney, J.F.B. Mitchell, R.J. Stouffer, and K.E. Taylor, 2007: The WCRP CMIP3 Multimodel Dataset: A new

era in climate change research. *Bull. Amer. Meteor. Soc.*, **88**, 1383–1394.

Met Office, cited 2008: Met Office: European heatwave 2003. [Available online at http://www.metoffice.gov.uk/education/secondary/students/european_heatwave/index.html.]

Molden, D., 2007: Water for food water for life: A comprehensive assessment of water management in agriculture. 48pp.

Morikawa, M., J. Morrison and P. Gleick, 2007: Corporate Reporting on Water: A review of eleven global industries [Hart, I. (ed)]. Pacific Institute for Studies in Development, Environment, and Security, Oakland, California, USA. 90pp.

Oregon State University, cited 2008: International Freshwater Treaties Database. [Available online at http://www.transboundarywaters.orst.edu/database/interfreshtreatdata.html.]

Palmer, W.C., 1965: Meteorological drought. Research Paper No. 45, U.S. Department of Commerce Weather Bureau, Washington, D.C.

Plummer, N., M.J. Salinger, N. Nicholls, R. Suppiah, K.J. Hennessy, R.M. Leighton, B. Trewin, C.M. Page, and J.M. Lough, 1999: Changes in climate extremes over the Australian region and New Zealand during the Twentieth Century. *Clim. Change*, **42**, 183–202.

Poveda, G. and O.J. Mesa, 1997: Feedbacks between hydrological processes in tropical South America and large-scale ocean–atmospheric phenomena. *J. Clim.*, **10**, 2690-2702.

Rind, D., R. Goldberg, J. Hansen, C. Rosenzweig, and R. Ruedy, 1990: Potential evapotranspiration and the likelihood of future drought. *J. Geophys. Res.*, **95**, 9983-

10,005.

Robock, A., K.Y. Vinnikov, C.A. Schlosser, N.A. Speranskaya, and Y. Xue, 1998: Evaluation of the AMIP soil moisture simulations. *Glob Planet Change*,**19**, 181–208.

Silvestri, G.E. and C.S. Vera, 2003: Antarctic Oscillation signal on precipitation anomalies over southeastern South America. *Geophys. Res. Lett.*, **30**, doi:10.1029/2003GL018277.

Stephenson, D.B., V. Pavan, M. Collins, M.M. Junge, and R. Quadrelli, 2006: North Atlantic Oscillation response to transient greenhouse gas forcing and the impact on European winter climate: A CMIP2 multi-model assessment. *Clim. Dyn.*, **27**, 401–420.

United Nations Office on Drugs and Crime, 2007: Colombia Coca Cultivation Survey for 2006.

U.S. Census Bureau, cited 2008: Census Bureau Home Page. [Available online at http://www.census.gov/.]

Varis, O., T. Kajander, and R. Lemmelä, 2004: Climate and water: from climate models to water resources management and vice versa. *Clim. Change*, **66**, 321–344.

Walter, K.M., S.A. Zimov, J.P. Chanton, D. Verbyla, and F.S. Chapin III, 2006: Methane bubbling from Siberian thaw lakes as a positive feedback to climate warming. *Nature*, **443**, 71-75.

Water: A shared responsibility: The United Nations World Water Development Report 2 (2006).

Webster, P.J., G.J. Holland, J.A. Curry, H.-R. Chang, 2005: Changes in tropical cyclone

number, duration and intensity in a warming environment. *Science*, **309**, 1844–1846.

Wetherald, R.T. and S. Manabe, 1999: Detectability of summer dryness caused by greenhouse warming. *Clim. Change*, **43**, 495-511.

Wittenberg, A.T., A. Rosati, N.-C. Lau, and J.J. Ploshay, 2006: GFDL's CM2 Global Coupled Climate Models. Part III: Tropical Pacific Climate and ENSO. *J. Clim.*, **19**, 698-722.

Wu, M.C., W.L. Chang, and W.M. Leung, 2004: Impacts of El Niño-Southern Oscillation events on tropical cyclone landfalling activity in the western North Pacific. *J. Clim.*, **17**, 1419–1428.

Yu, R., B. Wang, and T. Zhou, 2004: Tropospheric cooling and summer monsoon weakening trend over East Asia. *Geophys. Res. Lett.*, **31**, L22212, doi:10.1029/2004GL021270.

Zhai, P., X. Zhang, H. Wan, and X. Pan, 2004: Trends in total precipitation and frequency of daily precipitation extremes over China. *J. Clim.*, **18**, 1096–1108.

Zimov, S.A., E.A.G. Schuur, F.S. Chapin, 2006: Permafrost and the global carbon budget. *Science*, **312**, 1612-1613.

List of Figures

TABLE 1. This table shows the percentage of gridboxes in which five AOGCMs agree on the sign of the change between the last 20 years of the 20th and 21st centuries for the specified variables.

Precip	47.40%
Temp	100.00%
Soil Moisture	14.25%
SDDI	57.81%
Precip and Temp	36.44%
Precip and -(Temp)	10.96%
Precip and Soil Moisture	7.53%
Precip and -(Soil Moisture)	1.10%
Precip and SDDI	16.99%
Precip and -(SDDI)	2.05%
Temp and SDDI	6.16%
Temp and -(SDDI)	51.64%
Temperature and Soil Moisture	1.92%
Temp and -(Soil Moisture)	12.33%
Soil Moisture and SDDI	11.51%
Soil Moisture and -(SDDI)	0.27%

TABLE 2-8. These tables show IPCC AR4 scenario A2 model projections for changes in the average of the last 30 years of the 20th century and the last 30 years of the 21st century. Percentages are bases on the control period of 1928-1978. For SDDI and soil moisture, values in bold indicate drier conditions while values in regular typeface indicate wetter conditions. Both drought measures are displayed as the occurrence of late 21st century values in terms of their occurrence in the late 20th century. For example, in the Southwestern U.S. in JJA the model CCCMA, the average SDDI conditions in the years 2071-2100 occur only once every 2.27 years in the period 1971-2000.

Table 2: Southwestern U.S.

JJA	ΔT (°C)	ΔPr (mm/mo)	% of ctrl Pr	ΔCloud (%)	SDDI (1 in X ctrl yrs)	Soil (1 in X ctrl yrs)
cccma	4.56	0.72	2.3%	2.21	**2.27**	**1.08**
gfdl	6.18	-19.63	43.5%	-1.4	**6.16**	**1.59**
hadcm3	6.39	-3.63	9.0%	-0.99	**8.04**	**1.51**
miroc	6.54	-12.47	24.9%	-3.18	**23.88**	**5.22**
giss	4.54	-7.62	18.8%	2.17	**7.08**	**3.09**

DJF	ΔT (°C)	ΔPr (mm/mo)	% of ctrl Pr	ΔCloud (%)	SDDI (1 in X ctrl yrs)	Soil (1 in X ctrl yrs)
cccma	3.71	3.26	6.2%	-1.61	**1.75**	0.89
gfdl	3	-5.21	7.4%	-2.33	**4.22**	1.02
hadcm3	3.58	-3.42	4.9%	-2.87	**3.95**	-1.06
miroc	5.23	-6.66	12.3%	-3.74	**14.16**	**3.09**
giss	2.05	-4.29	6.2%	-3.62	**2.96**	**1.16**

Table 3: Southern Europe

JJA	ΔT (°C)	ΔPr (mm/mo)	% of ctrl Pr	ΔCloud (%)	SDDI (1 in X ctrl yrs)	Soil (1 in X ctrl yrs)
cccma	5.06	-15	25.2%	-11.16	**4.55**	**1.66**
gfdl	5.3	-28.61	57.1%	-12	**12.44**	**2.04**
hadcm3	6.63	-26.21	41.2%	-13.59	**7.03**	**2.52**
miroc	5.62	3.17	5.8%	-6.98	**5.18**	**2.17**
giss	4.87	-18.54	27.5%	-3.35	**5.56**	**4.71**

DJF	ΔT	ΔPr	% of ctrl Pr	ΔCloud (%)	SDDI (1 in X ctrl yrs)	Soil (1 in X ctrl yrs)
cccma	3.51	5.52	9.5%	-0.44	**3.47**	**1.02**
gfdl	2.53	-4.92	6.4%	-4.47	**8.60**	**1.12**
hadcm3	3.29	6.85	9.4%	-0.43	**5.28**	**1.13**
miroc	3.32	0.62	1.0%	-3.96	**5.64**	**1.59**
giss	3.09	5.61	7.3%	-1.61	**3.39**	**1.20**

Table 4: Uruguay

JJA	ΔT (°C)	ΔPr (mm/mo)	% of ctrl Pr	ΔCloud (%)	SDDI (1 in X ctrl yrs)	Soil (1 in X ctrl yrs)
cccma	2.94	2.77	3.8%	-2.25	**1.56**	1.17
gfdl	2.41	-6.48	28.5%	-1.55	**2.11**	**1.20**
hadcm3	3.03	-3.35	7.5%	-6.8	**3.73**	1.03
miroc	2.22	-2.17	14.0%	3.27	**7.20**	1.42
giss	1.49	0.99	14.7%	1.68	**1.04**	1.24

DJF	ΔT (°C)	ΔPr (mm/mo)	% of ctrl Pr	ΔCloud (%)	SDDI (1 in X ctrl yrs)	Soil (1 in X ctrl yrs)
cccma	2.79	29.04	22.4%	4.44	**1.32**	2.74
gfdl	2.57	10.14	10.5%	0.58	**3.34**	1.09
hadcm3	3.16	6.31	7.2%	-2.83	**3.42**	1.25
miroc	2.33	18.86	22.3%	1.46	**3.31**	1.75
giss	3.14	1.27	4.0%	0.45	**5.44**	**0.83**

Table 5: Colombia

JJA	ΔT (°C)	ΔPr (mm/mo)	% of ctrl Pr	ΔCloud (%)	SDDI (1 in X ctrl yrs)	Soil (1 in X ctrl yrs)
cccma	3.96	-5.94	4.6%	-3.5	**3.78**	**1.14**
gfdl	4.14	-6.44	6.1%	-1.64	**1.88**	**1.25**
hadcm3	6.25	-35.85	27.4%	-12.21	**4.54**	**1.30**
miroc	4.28	-7.34	6.5%	-5.08	**2.96**	**1.18**
giss	2.85	23.17	13.7%	7.56	**1.07**	**0.77**

DJF	ΔT (°C)	ΔPr (mm/mo)	% of ctrl Pr	ΔCloud (%)	SDDI (1 in X ctrl yrs)	Soil (1 in X ctrl yrs)
cccma	3.74	19.75	18.5%	-0.12	**2.93**	**1.00**
gfdl	2.95	32.99	27.0%	2.57	**1.75**	**0.89**
hadcm3	4.85	-1.49	1.1%	-6.1	**7.80**	**1.12**
miroc	3.75	18.92	16.8%	1.95	**3.91**	**1.02**
giss	3.01	21.56	12.4%	-1.73	**1.04**	1.20

Table 6: Eastern China

JJA	ΔT (°C)	ΔPr (mm/mo)	% of ctrl Pr	ΔCloud (%)	SDDI (1 in X ctrl yrs)	Soil (1 in X ctrl yrs)
cccma	3.55	30.72	16.6%	-3.26	1.14	1.24
gfdl	4.43	17.2	9.8%	-2.23	**1.32**	0.92
hadcm3	4.41	24.16	13.4%	-1.75	0.92	1.32
miroc	3.8	1.24	0.8%	-3.88	**1.54**	**1.16**
giss	2.73	31.51	12.4%	0.81	1.00	1.06

DJF	ΔT (°C)	ΔPr (mm/mo)	% of ctrl Pr	ΔCloud (%)	SDDI (1 in X ctrl yrs)	Soil (1 in X ctrl yrs)
cccma	3.96	5.39	13.7%	0.46	**0.86**	1.01
gfdl	3.15	-0.95	3.8%	-3.28	**1.99**	**1.28**
hadcm3	4.18	10.73	35.1%	2.31	**1.08**	1.10
miroc	4.19	1.06	4.1%	0.72	**1.53**	**1.17**
giss	3.43	9.22	12.9%	-1.53	**0.92**	**0.91**

Table 7: Eastern Siberia

JJA	ΔT (°C)	ΔPr (mm/mo)	% of ctrl Pr	ΔCloud (%)	SDDI (1 in X ctrl yrs)	Soil (1 in X ctrl yrs)

cccma	3.97	3.71	9.0%	-0.4	**1.18**	**1.59**
gfdl	1.73	13.19	30.0%	2.33	1.18	**1.46**
hadcm3	4.61	10.18	17.2%	-3.92	1.03	**1.35**
miroc	5	8.8	12.6%	-6.13	**0.86**	**1.13**
giss	2.76	3.01	7.1%	-1.91	**0.90**	0.86

DJF	ΔT (°C)	ΔPr (mm/mo)	% of ctrl Pr	ΔCloud (%)	SDDI (1 in X ctrl yrs)	Soil (1 in X ctrl yrs)
cccma	7.11	4.97	46.7%	11.44	1.07	**1.23**
gfdl	8.63	7.41	63.1%	0.36	2.55	1.11
hadcm3	8.61	7.41	70.7%	0.62	1.38	1.02
miroc	8.98	7.02	60.7%	3.12	1.28	1.20
giss	4.51	5.46	27.8%	0.97	1.22	**0.98**

Table 8: Australia

JJA	ΔT (°C)	ΔPr (mm/mo)	% of ctrl Pr	ΔCloud (%)	SDDI (1 in X ctrl yrs)	Soil (1 in X ctrl yrs)
cccma	3.09	9.26	36.5%	5.41	**2.34**	1.28
gfdl	3.28	-6.75	31.6%	-6	**5.13**	**1.42**
hadcm3	3.38	-3.42	15.2%	-2.72	**5.00**	1.17
miroc	3.26	2.02	6.1%	-1.84	**4.16**	1.27
giss	4.26	-5.78	19.6%	-8.5	**3.66**	**1.64**

DJF	ΔT (°C)	ΔPr (mm/mo)	% of ctrl Pr	ΔCloud (%)	SDDI (1 in X ctrl yrs)	Soil (1 in X ctrl yrs)
cccma	4.1	8.86	20.1%	-0.2	**5.45**	**0.89**
gfdl	3.6	-14.13	12.8%	-4.01	**5.41**	**1.14**
hadcm3	4.1	-7.48	7.7%	-4.65	**6.97**	1.05
miroc	3.33	10.78	9.3%	-0.85	**4.32**	1.01
giss	3.42	4.92	4.0%	-2.23	**5.30**	**1.10**

TABLE 9a. This table lists annual best-fit multiple linear regression coefficients for 1901-2100 from equations 1 and 2 for both drought measures in each region and model.

$|\beta_T/\beta_{PR}| > 1$ indicates situations in which temperature has a larger influence than precipitation on the drought measure. The r^2 values represent the proportion of variability in the model output that is accounted for by the linear equation.

Annual Soil Moisture Regression
Southwestern United States

Model	β_C	β_T	β_{PR}	β_T/β_{PR}	r^2
cccma	0.66	0.38	1.58	0.24	0.36
gfdl	0.46	-0.60	0.67	-0.90	0.81
giss	-0.07	-7.80	1.51	-5.15	0.73
hadcm	-1.62	-1.32	2.16	-0.61	0.58
miroc	7.20	-32.75	2.38	-13.77	0.80

Annual SDDI Regression
Southwestern United States

Model	β_C	β_T	β_{PR}	β_T/β_{PR}	r^2
cccma	0.01	-0.58	0.09	-6.58	0.84
gfdl	-0.08	-0.70	0.07	-10.02	0.87
giss	-0.04	-0.96	0.08	-11.74	0.90
hadcm	-0.10	-0.70	0.08	-8.41	0.89
miroc	0.06	-0.95	0.09	-10.73	0.90

Southern Europe

Model	β_C	β_T	β_{PR}	β_T/β_{PR}	r^2
cccma	3.26	-2.12	2.06	-1.03	0.66
gfdl	1.19	-1.60	0.65	-2.47	0.90
giss	-2.47	-8.27	1.70	-4.86	0.78
hadcm	-0.65	-5.51	1.70	-3.24	0.83
miroc	1.90	-24.52	2.58	-9.50	0.80

Southern Europe

Model	β_C	β_T	β_{PR}	β_T/β_{PR}	r^2
cccma	0.12	-1.02	0.10	-10.74	0.90
gfdl	0.01	-1.28	0.09	-13.51	0.90
giss	-0.21	-0.80	0.10	-8.41	0.90
hadcm	0.04	-0.97	0.07	-13.29	0.90
miroc	0.17	-1.07	0.12	-8.72	0.90

Uruguay

Model	β_C	β_T	β_{PR}	β_T/β_{PR}	r^2
cccma	0.67	-1.32	2.42	-0.55	0.59
gfdl	0.32	-1.05	0.74	-1.42	0.86
giss	-0.85	0.57	1.56	0.36	0.51
hadcm	-0.30	-0.86	2.41	-0.36	0.63
miroc	14.09	28.35	4.49	6.31	0.50

Uruguay

Model	β_C	β_T	β_{PR}	β_T/β_{PR}	r^2
cccma	-0.11	-1.09	0.09	-12.64	0.68
gfdl	-0.13	-1.44	0.06	-24.57	0.74
giss	-0.01	-1.10	0.08	-14.70	0.88
hadcm	-0.10	-1.24	0.07	-17.00	0.74
miroc	0.06	-1.76	0.08	-22.04	0.80

Colombia

Model	β_C	β_T	β_{PR}	β_T/β_{PR}	r^2
cccma	0.32	-1.55	0.68	-2.27	0.66
gfdl	0.59	-1.82	0.34	-5.38	0.90
giss	0.82	-6.64	1.59	-4.17	0.45
hadcm	-0.29	0.85	1.17	0.72	0.82
miroc	8.28	-15.32	2.19	-7.01	0.50

Colombia

Model	β_C	β_T	β_{PR}	β_T/β_{PR}	r^2
cccma	0.05	-1.07	0.03	-37.93	1.00
gfdl	0.16	-0.85	0.01	-82.12	0.70
giss	-0.10	-0.91	0.08	-11.22	0.80
hadcm	-0.06	-1.12	0.02	-59.62	0.90
miroc	0.02	-1.01	0.05	-19.60	0.90

Eastern China

Model	β_C	β_T	β_{PR}	β_T/β_{PR}	r^2
cccma	-0.67	-3.64	1.18	-3.08	0.51

Eastern China

Model	β_C	β_T	β_{PR}	β_T/β_{PR}	r^2
cccma	0.04	-0.26	0.06	-4.05	0.50

gfdl	0.96	-1.49	0.59	-2.52	0.70
giss	-0.68	-0.81	0.92	-0.88	0.52
hadcm	2.42	-3.08	1.10	-2.80	0.37
miroc	8.44	-16.70	2.42	-6.90	0.60

gfdl	-0.08	-0.63	0.07	-9.18	0.80
giss	0.02	-0.20	0.04	-4.47	0.50
hadcm	-0.04	-0.37	0.06	-5.83	0.50
miroc	0.04	-0.59	0.08	-7.79	0.80

Eastern Siberia

Model	β_C	β_T	β_{PR}	β_T/β_{PR}	r^2
cccma	1.83	-2.53	1.10	-2.30	0.39
gfdl	0.38	-0.90	0.73	-1.23	0.30
giss	1.13	-1.08	0.68	-1.59	0.14
hadcm	2.96	-2.79	1.59	-1.75	0.17
miroc	-2.95	-1.29	1.12	-1.16	0.10

Eastern Siberia

Model	β_C	β_T	β_{PR}	β_T/β_{PR}	r^2
cccma	0.11	-0.31	0.33	-0.93	0.40
gfdl	0.03	-0.04	0.23	-0.16	0.80
giss	0.05	-0.12	0.21	-0.58	0.60
hadcm	0.05	-0.18	0.23	-0.78	0.50
miroc	-0.16	-0.21	0.21	-1.00	0.50

Australia

Model	β_C	β_T	β_{PR}	β_T/β_{PR}	r^2
cccma	0.06	-0.29	1.24	-0.23	0.78
gfdl	0.05	-0.62	0.32	-1.92	0.90
giss	-0.38	-2.22	1.00	-2.21	0.53
hadcm	0.34	2.83	1.52	1.86	0.49
miroc	11.64	-1.30	3.64	-0.36	0.30

Australia

Model	β_C	β_T	β_{PR}	β_T/β_{PR}	r^2
cccma	-0.04	-1.02	0.05	-20.67	0.90
gfdl	0.05	-1.34	0.04	-32.89	0.90
giss	0.03	-1.12	0.04	-27.13	0.90
hadcm	0.10	-1.37	0.01	-113.81	0.90
miroc	0.21	-1.39	0.06	-22.90	0.80

TABLE 9b. This table lists JJA and DJF best-fit multiple linear regression coefficients for 1901-2100 from equations 1 and 2 for both drought measures in each model for the

Southwestern U.S. $|\beta_T/\beta_{PR}| > 1$ indicates situations in which temperature has a larger influence than precipitation on the drought measure. The r^2 values represent the proportion of variability in the model output that is accounted for by the linear equation.

Southwestern United States

JJA Soil Moisture Regression

Model	β_C	β_T	β_{PR}	β_T/β_{PR}	r^2
cccma	0.55	-0.41	0.87	-0.46	0.20
gfdl	-0.35	-0.63	0.44	-1.43	0.91
giss	0.98	-9.34	0.55	-16.98	0.75
hadcm	-1.18	-3.50	0.90	-3.91	0.50
miroc	4.73	-30.78	1.07	-28.85	0.90

JJA SDDI Regression

Model	β_C	β_T	β_{PR}	β_T/β_{PR}	r^2
cccma	0.07	-0.53	0.03	-17.66	0.75
gfdl	0.04	-0.57	0.04	-13.94	0.86
giss	0.03	-0.88	0.02	-35.44	0.90
hadcm	-0.11	-0.63	0.04	-17.50	0.84
miroc	-0.03	-0.91	0.04	-21.71	0.90

DJF Soil Moisture Regression

Model	β_C	β_T	β_{PR}	β_T/β_{PR}	r^2
cccma	1.31	1.39	0.69	2.00	0.27
gfdl	2.32	-1.45	0.46	-3.13	0.35
giss	-4.18	-3.91	0.84	-4.63	0.37
hadcm	-4.77	-0.32	1.03	-0.31	0.45
miroc	-4.21	-30.46	0.64	-47.58	0.60

DJF SDDI Regression

Model	β_C	β_T	β_{PR}	β_T/β_{PR}	r^2
cccma	-0.14	-0.47	0.04	-13.23	0.58
gfdl	-0.57	-0.67	0.03	-20.36	0.47
giss	-0.59	-0.69	0.04	-15.86	0.45
hadcm	-0.53	-0.65	0.04	-16.98	0.61
miroc	-0.24	-0.87	0.04	-24.49	0.72

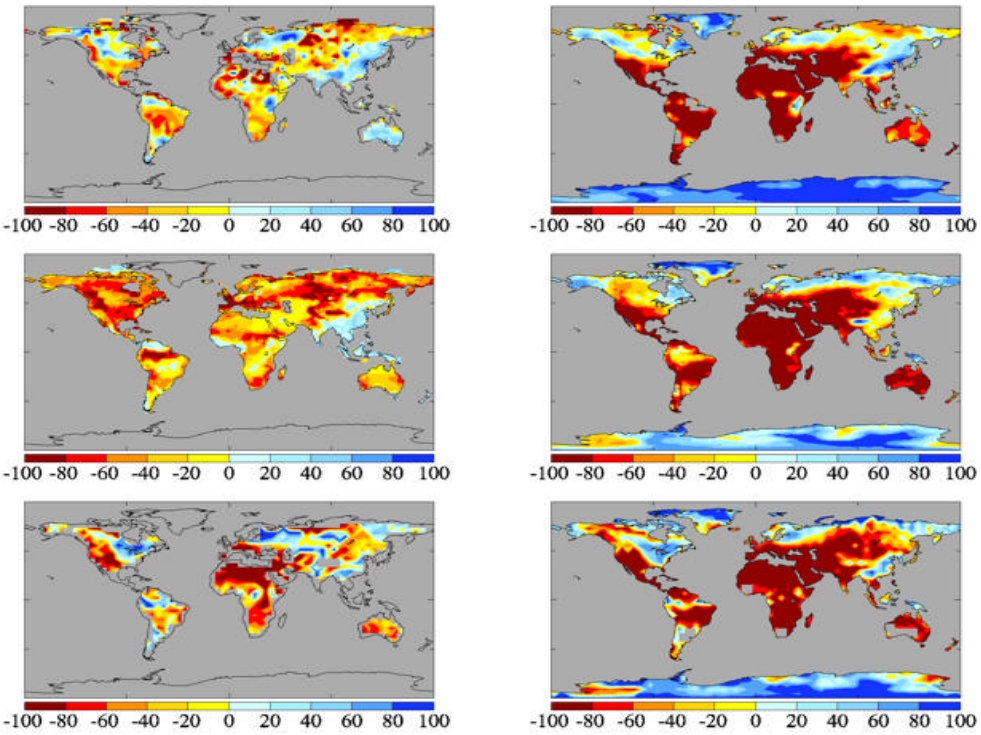

FIG. 1. Extremes of averaged June-August water availability in the last 30 years of the 21st century with respect to the control period (1928-1978) for both soil moisture (left) and SDDI (right). Results are shown as a percentage of time during which the 2071-2100 June-August average conditions occurred during the control period of 1928-1978 [e.g., deep red (-100% to -80%) indicates dry conditions of this magnitude happened less than 20% of the time in the control period for that grid box]. Positive (negative) values indicate fluvial (drought) conditions. Projections from 3 AOGCMs are displayed (top: CCCMA, middle: GFDL, bottom: GISS).